



ELSEVIER

Available online at www.sciencedirect.com

SCIENCE @ DIRECT®

Nuclear Instruments and Methods in Physics Research A 497 (2003) 90–97

**NUCLEAR
INSTRUMENTS
& METHODS
IN PHYSICS
RESEARCH**
Section A

www.elsevier.com/locate/nima

Factors affecting cancer detectability in ^{99}Tc MIBI scintimammography

R. Pani^{a,*}, R. Pellegrini^a, G. De Vincentis^a, M.N. Cinti^a, I.N. Weinberg^b,
A. Soluri^c, A.M. Betti^a, F. Scopinaro^a, M. Marini^a, R. Massa¹, N. Lanconelli^d,
A. Riccardi^d, F. Garibaldi^e

^aDepartment of Experimental Medicine and Pathology, University of Rome "La Sapienza", Viale Regina Elena 324, 00161 Rome, Italy

^bPEM Technologies, Bethesda, MA, USA

^cInstitute of Biomedical Technologies, CNR, Rome, Italy

^dDepartment of Physics, University of Bologna, Italy

^eLaboratory of Physics, ISS, Rome, Italy

Abstract

Scintimammography shows strong potential in detecting and differentiating breast cancer. This scintigraphic technique, using a standard gamma camera, allows high sensitivity and specificity values (>95%) for detected tumors more than 1 cm size. However, the sensitivity of scintimammography using conventional gamma cameras is considerably less (40–50%) for tumors with smaller size. Recently, the authors demonstrated how the use of a small FOV dedicated gamma camera (Single Photon Emission Mammography, or SPEM camera), with very high intrinsic spatial resolution (1.7 mm FWHM), working with breast moderately compressed and positioned close to the breast tumor (i.e., analogously to X-ray mammography) increased sensitivity up to 80% for tumors sized between 0.5 and 1 cm (T1b). The aim of this paper is to demonstrate how the reduced breast thickness can play a primary role in small cancer detection. Five different methods were taken into account: clinical measurements, comparing tumor SNR values obtained from the same patients in prone scintimammography and in SPEM, comparing SNR values between compressed and uncompressed breast in craniocaudal projection, breast phantom measurements, Monte Carlo simulations and simplified theoretical model. Results confirm that the mechanism for the improvement in visualizing sub-centimeter lesions due to compression is a reduction of lesion–detector distance. As a result of this reduced distance there is a less reabsorption of signal by interposed breast tissue, and improved detector intrinsic spatial resolution.

© 2002 Elsevier Science B.V. All rights reserved.

PACS: 29.40.M; 29.25.R; 87.50.N

Keywords: Scintimammography; Radiotracer; MIBI; $^{99\text{m}}\text{Tc}$; Nuclear medicine imaging

1. Introduction

Diagnosis and treatment of cancer at early stage of development increases outlook of long-term survival.

*Corresponding author. Tel.: +39-6-49918277; fax: +39-6-49918277.

E-mail address: roberto.pani@uniroma1.it (R. Pani).

Currently, X-ray mammography represents the principal method of detecting breast cancer. Unfortunately, X-ray mammography is not an ideal examination, because its diagnostic accuracy is below 100% and therefore many patients are submitted to unnecessary biopsies. Several studies estimated that only 10–40% of all biopsies performed on the basis of X-ray mammography are positive. Therefore, improvement in patient comfort and health care costs can be achieved if some of these unnecessary biopsies are avoided.

We believe that some unnecessary biopsies can be avoided by exploiting capabilities of ^{99m}Tc -MIBI Scintimammography (SM) [1,2]. Previous works have demonstrated that ^{99m}Tc -MIBI is preferentially taken up by cells with characteristics of malignancy due to increased metabolic turnover. The present standard scintimammographic technique was introduced for the first time by Khalkhali in 1993 [1]. It is named Prone ScintiMammography (PSM). It consists of positioning a gamma camera in lateral view of body with the patient in prone position and the breast pendulant. It was recently shown as, by combining results from X-ray mammography and SM, a significant increase of diagnostic accuracy was achieved [3]. We would like to further increase the improvement by increasing the sensitivity of SM to lesions with diameter less than 1 cm (T1a and T1b cancers).

Our group has been the first to conceive and realize a high spatial resolution detector specifically dedicated to SM, the Single Photon Emission Mammography (SPEM) [4–7] camera. This camera uses position sensitive photomultiplier tubes, coupled to an array of scintillating crystal. Other detectors for SM have been considered for commercial applications [8–11]. The examination by SPEM camera is typically performed in craniocaudal view, with the breast moderately compressed. Clinical results with this SPEM camera have demonstrated an increase of diagnostic sensitivity of SM in T1b tumors (80% vs. 50% with PSM) [12–18], while the results obtained in smaller lesions (T1a) remain unsatisfactory. The aim of this paper is to demonstrate how the reduced breast thickness can play a primary role in

small cancer detection. Five different methods were taken into account:

1. clinical measurements, comparing tumor SNR values obtained from the same patients in prone scintimammography and in SPEM, comparing SNR values between compressed and uncompressed breast in craniocaudal projection;
2. breast phantom measurements;
3. Monte Carlo simulations;
4. simplified theoretical model.

2. Equipment and method

2.1. Clinical measurements

A standard gamma camera (GE Starcam) and a SPEM camera were utilized for image acquisition. The SPEM camera consists of a 5" Position Sensitive PhotoMultiplier Tube (Hamamatsu R3292) coupled to a CsI(Tl) scintillating array where each individual pixel is $2 \times 2 \times 3 \text{ mm}^3$ in size. A detailed description of the SPEM camera is reported elsewhere [4,7]. All purpose collimators were used for both cameras: a GE H2503DF with 2.5 mm hole diameter, 41 mm hole length, 0.3 mm septa, and a Nuclear Fields collimator with 1.5 mm hole diameter, 22 mm hole length, 0.2 mm septa, respectively. Both collimators, currently utilized for breast clinical measurements, allow approximately the same spatial resolution values, but different sensitivity values: 362 and 600 cpm/ μCi (for GE and Nuclear Fields, respectively). A breast/torso phantom was placed in front of both collimators to analyze the influence on SNR of breast thickness and different intrinsic spatial resolution (3.5 and 1.7 mm FWHM) and energy resolution values (10% and 20% FWHM) of GE and SPEM cameras, respectively. The energy resolution values for SPEM Camera were obtained after a correction of pulse height uniformity response, using a lookup table based on the spectra acquired on each pixel of the digitalized image.

To analyze the improvement introduced by SPEM gamma camera, the same patients were imaged by prone SM and SPEM, respectively.

Breast images and tumor SNR values were then compared. Furthermore, some patients were imaged with breast compressed and uncompressed under craniocaudal projection in SPEM obtaining 7.5 ± 0.5 cm and 5.0 ± 0.2 cm mean thickness values, respectively.

Fourteen patients were enrolled for in vivo measurements, where five patients with breast tumors sized between 5 and 7 mm, were correctly diagnosed with the SPEM camera, as compared to ($\frac{2}{3}$) by prone SM. The results have been analyzed, using the histological findings as a gold standard.

3. High spatial resolution detector

To evaluate if tumor detectability could be improved by an imager with very high spatial resolution, a small gamma camera with higher performance than SPEM was specifically assembled. It is based on pixellated detector being able to carry out images with a very good crystal pixel identification and allowing an effective correction of the spatial response. This Small Gamma Camera (SGC) was arranged using a metal channel dynode position sensitive photomultiplier (Hamamatsu R7600–C8) [8,9] coupled to different CsI(Tl) scintillator arrays and with the same SPEM collimator. This kind of photomultiplier drastically reduces the charge spread improving performance of the imager. The dimension of the CsI(Tl) arrays were the same of the photomultiplier active area (22×22 mm²). To realize the very high intrinsic spatial resolution, a look-up table was employed to accurately correct the gain and spatial non-uniformities. To study the potential dependence of crystal pixel size on tumor SNR, a number of CsI (Tl) scintillating arrays were tested. Crystals were 5 mm thick, dead zone was 0.25 mm thick, and single crystal side ranged between 2.0 and 4.2 mm. The SGC camera readout is made of eight preamplifiers directly connected to each wire anode. A weighted summing circuit was built to compute the charge distribution centroid. The acquisition system consists of a 7074 Quad ADC module connected to a multiparameter FAST MPA/WIN. The MPA acquisition card is plugged in a PC/Pentium [8,9].

4. Phantom studies

To perform a SNR analysis of different tumor size, a breast/torso phantom was built. It consists of a cylinder with 9 cm diameter and 15 cm height, filled with technetiated water at 3, 6 and 9 cm to simulate different breast compression thickness. Three tumor sizes were taken into account, corresponding to the clinical staging criteria of T1b (greater than 5 mm, less than or equal to 1 cm) and T1c. The T1b hot spots were 6 mm and 8 mm diameter cylinders with 0.5 cc volume. The T1c (10 mm diameter) had 1 cc volume. The tumor depth was 0.5 and 3 cm (Source Collimator Distance—SDC). A box of $30 \times 30 \times 20$ cm³, also filled with technetiated water, was placed close to the breast phantom to simulate the torso emission (see Fig. 1). Radioactivity concentration values were chosen to obtain about the 1:1 torso:breast ratio of clinical image (100 nCi/cc concentration). About the tumor phantom we used for the tumor–breast ratio (tum/bck) 10:1 for 6 and 8 mm tumor while 8:1 for 10 mm tumor.

A craniocaudal projection was simulated as function of different breast thickness with tumors in a fixed position. We are aware that this experimental set up does not correspond to the usual Anger camera scintimammographic technique (PSM), but it would further enhance Anger camera imaging performance by reducing tumor-to-collimator distances to better evaluate the

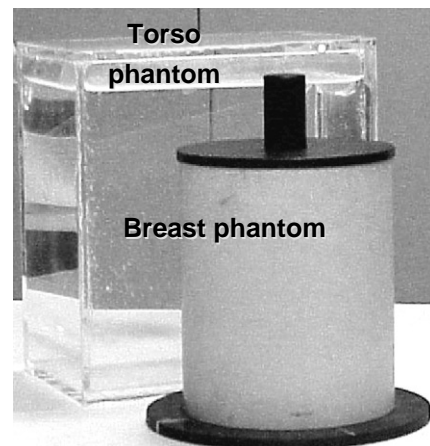


Fig. 1. Breast phantom.

advantages offered by dedicated detectors. Image acquisition conditions were the same as during SPEM clinical measurements and radioactivity concentration values were chosen to obtain about the same pixel count of clinical images.

4.1. Breast phantom simulation

The breast phantom was fully simulated as well as all interaction processes in the gamma camera. The Monte Carlo code used is EGSnrc, the latest version of the EGS family. Simulations include all the physical processes available with EGS, as Compton and Rayleigh scattering, photoelectric absorption with emission of fluorescence photons or Auger electrons. In order to emulate a clinical examination, the number of simulated photons was calculated from an imaging time of 10 min and a background activity of 100 nCi/cc. We simulated three different spherical tumors (5, 8, 10 mm diameter), located at various depths (0.5, 3 cm from the collimator); the tum/bck considered was 10:1. Unlike the experimental phantom measurements, here tumor volumes scaled with spherical ones. The simulated camera included the same SGC lead collimator and CsI-pixelated crystals.

4.2. Geometrical model

To further evaluate the influence of gamma camera positioning on tumor SNR values with respect to gamma energy transport, a simple mathematical model was performed. Tumor radioactivity amount is assumed strictly related to the tumor size (sphere volume) as for Monte Carlo simulation. ROI tumor is related to geometrical projection only, of the tumor on the image, taking into account intrinsic spatial resolution of the gamma camera, collimator characteristics, tumor to collimator distance and image pixellation.

5. Results and conclusions

The results of clinical data are shown in Figs. 2 and 3. The SNR values obtained by SPEM with breast compressed in craniocaudal projection are higher than prone SM of about a factor two. In

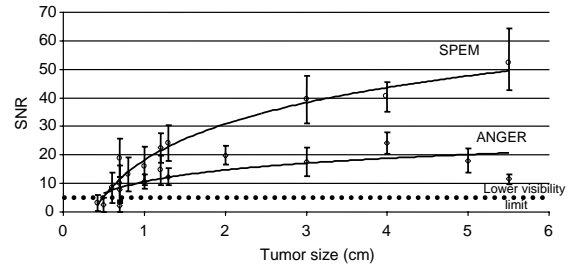


Fig. 2. Tumor SNR values obtained from clinical measurements by SPEM camera (craniocaudal projection) and Anger camera (PSM), respectively.

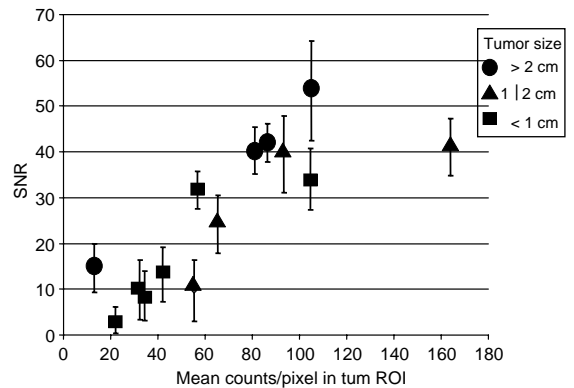


Fig. 3. mean counts values per image pixel calculated on tumor ROIs imaged by SPEM.

particular, tumors less than 1 cm sized, imaged by SPEM, show SNR values largely distributed over the visibility limit (SNR = 5), between 7 and 20. On the contrary, prone SM tumor SNR values ranged between 3 and 10 confirming the lack of sensitivity for tumors less than 1 cm in size. Fig. 3 shows an interesting analysis about the mean counts on image pixel obtained from the selected tumor ROIs. The breast compression values ranged between 4 and 5 cm. In the figure, values are grouped for three different tumor sizes. It is worthy to note how all values show approximately the same variation range (i.e. between 10 and 40 mean counts/pixel for an image pixel size of 2.5 mm × 2.5 mm). This demonstrates the critical resolution and sensitivity requirements. Furthermore, compression allows the separation of overlapped objects as it is clearly visible in the images shown in Fig. 4 on 7 mm tumor detection. A

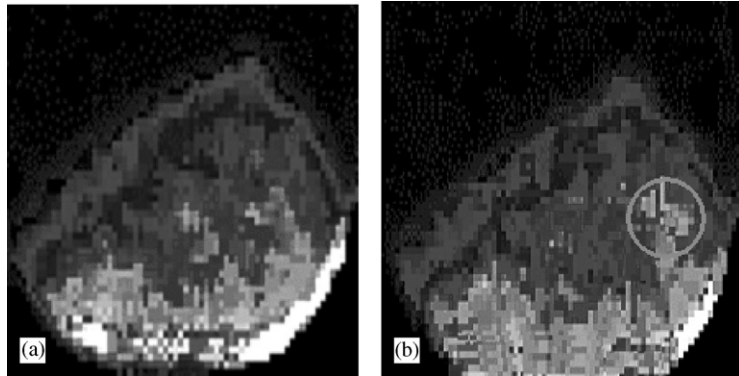


Fig. 4. Right breast carcinoma 7 mm sized: SPEM camera ^{99m}Tc Sestamibi Scintimammograms with uncompressed breast (left) and mildly compressed (right). Into the circle the lesion is shown as a more enhanced area of increased uptake of tracer.

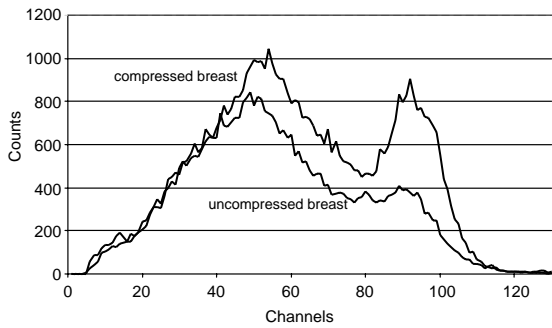


Fig. 5. Energy spectrum from the same tumor ROI of compressed and uncompressed breast. Tumor size: 5.5 cm, uncompressed breast size: 22 cm (w) \times 13 cm (l) \times 10 cm (h), SNR = 12; compressed breast size: 22 cm (w) \times 13 cm (l) \times 5.5 cm (h), SNR = 25.

further analysis on the effectiveness of breast compression is in Fig. 5 where the detected spectra are shown respectively. In this case the large tumor size combined with the large variations in breast thickness (4.5 cm) show an impressive counting increasing of the signal (full energy peak) with respect to Compton background.

The results of breast phantom analysis, obtained by SGC camera with different crystal pixel size are shown in Figs. 6–8, in comparison with the analogous ones obtained by Anger Camera and by Monte Carlo simulations. The analysis took into account only the craniocaudal breast projection at 3 and 6 cm breast compression values. Tumor SNR values obtained by Anger camera are

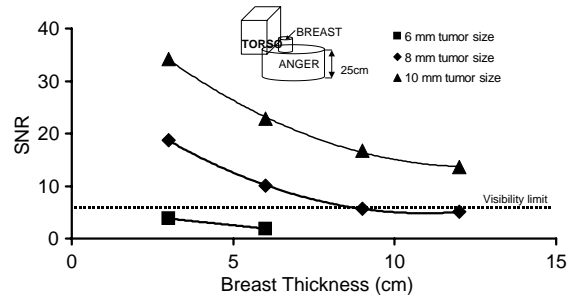


Fig. 6. Breast phantom measurements by Anger camera in craniocaudal projection. 2.5 cm tumor–detector–distance.

drawn as a function of breast thickness. As shown in Fig. 6 the breast thickness at a fixed tumor–detector distance reduces the tumor visibility down to more than a factor two. Furthermore, taking into account that tumors mostly differ in size than in the amount of radioactivity, SNR values resulted strongly affected by Anger camera spatial resolution. In fact, the 6 mm tumor resulted under the visibility limit, differing up to a factor four with respect to the 8 mm tumor SNR at the same breast thickness. The results of SNR values as function of tumor size are shown in Figs. 7 and 8. The results obtained by SGC and by Monte Carlo simulation are less affected by the noise introduced from the breast thickness. Results confirm how detector spatial resolution and tumor to collimator distance play a fundamental role in small tumor detection. In fact, the 6 mm tumor visibility

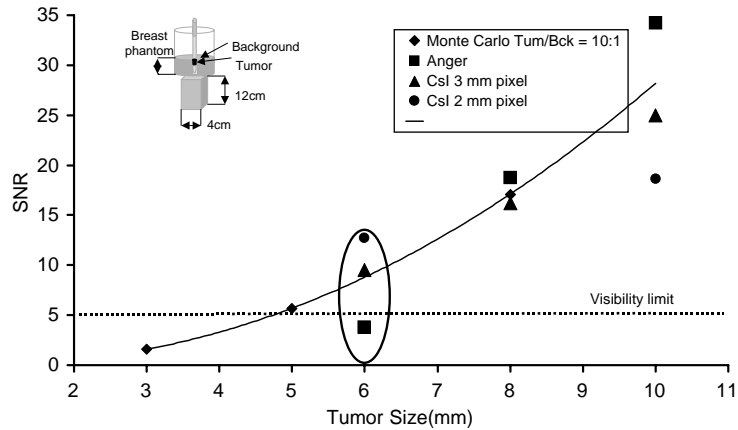


Fig. 7. Breast phantom measurements: tumor SNR values obtained at 2.5 cm tumor–detector–distance and 3 cm breast thickness.

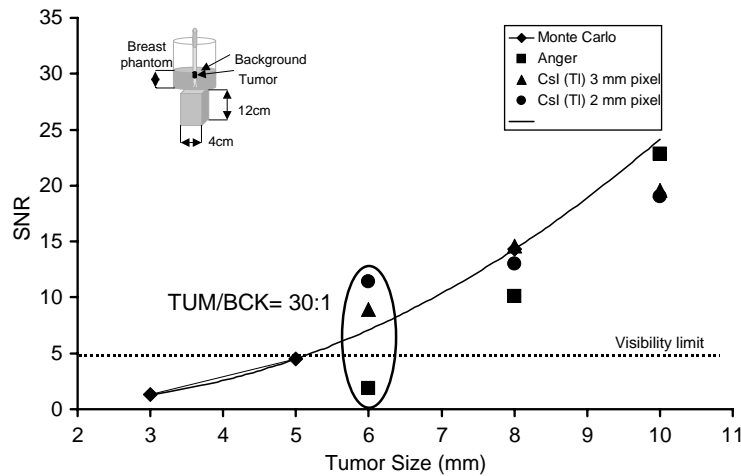


Fig. 8. Breast phantom measurements: tumor SNR values obtained at 2.5 cm tumor–detector–distance and 6 cm breast thickness.

improved more than four times by SGC and in particular reducing the crystal pixel size. The Monte Carlo results roughly confirm the values obtained by SGC taking into account the different tumor radioactivity amount between theoretical and experimental phantom. It shows also how 5 mm tumor is at visibility limit when located at 3 cm depth.

The results obtained by geometrical model confirm the clinical data about sensitivity, In fact as shown in Fig. 9, prone SM is able to carry out SNR values greater than 5 only for tumor size greater than 1 cm. Fig. 10 shows good SNR values

for T1b tumors only at breast thickness values less than 4–5 cm when imaged by a gamma camera with very high intrinsic spatial resolution (less than 2 mm intrinsic spatial resolution and the same collimator used in SPEM and SGC). Furthermore, Fig. 10 shows how it is critical the detection of tumor less than 5 mm size for breast thickness greater than 2.5 cm and at tumor–collimator distance coinciding with this value. The SNR is always under the visibility limit.

In conclusion, the adoption of breast compression with a dedicated imager can allow: improved detector spatial resolution by reducing tumor to

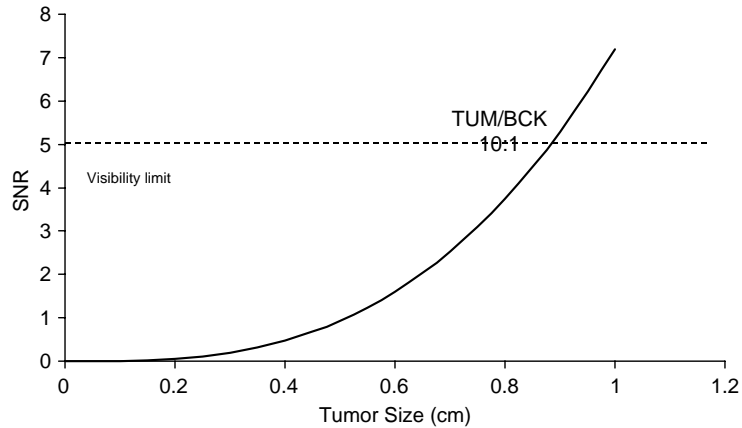


Fig. 9. geometrical model (no radiation transport) simulating PSM by Anger Camera. Tumor to detector distance = 10 cm, Breast thickness = 13 cm.

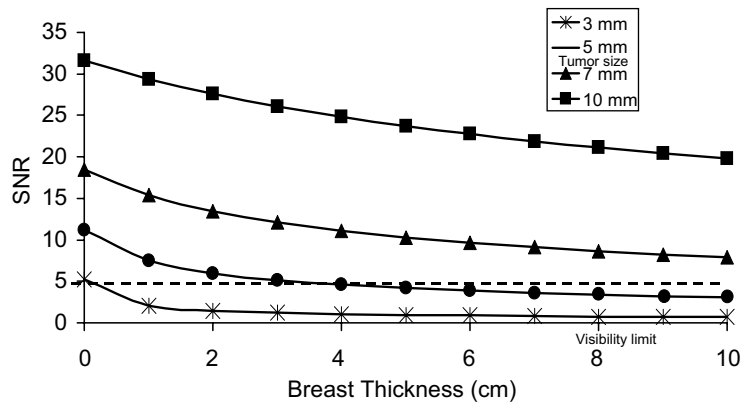


Fig. 10. geometrical model (no radiation transport) simulating a craniocaudal projection, a tumor to collimator distance of 2.5 cm and a 2 mm × 2 mm pixellated detector (SGC).

collimator distance; improved subject contrast by reducing background radioactivity and single and multiple photon scattering into the breast; improved image statistics by reducing gamma ray self-absorption into the breast; diminished motion unsharpness due to breast immobilization; and separation of overlapped objects and more uniform image.

Spot compression allows a further reduction of the breast thickness with respect to the average value obtained from vigorous compression in RX mammography (4.4 cm in craniocaudal projection). Spot compression allows to overcome the limitation offered from the long acquisition time

(10 min) in SPEM and the consequent use of the breast moderate compression to avoid patient discomfort. Skin elasticity is the primary limit to breast compressibility and it is responsible of pain during RX mammography. Reducing the compression area it is possible to achieve a higher compression with the minimum patient discomfort. X-ray mammography is currently applying the spot compression to enhance contrast and sensitivity of small lesions. The research group considers the combining spot compression/dedicated small FOV gamma camera the primary goal to improve the sensitivity of scintimammography for small tumors.

References

- [1] I. Khalkali, I. Mena, E. Jouanna, et al., *J. Am. Coll. Surg.* 78 (1994) 491.
- [2] F. Scopinaro, O. Schillaci, M. Scarpini, et al., *Eur. J. Nucl. Med.* 21 (9) (1994) 984.
- [3] Buscombe, et al., *J. Nucl. Med.* 42 (1) (2001) 3.
- [4] R. Pani, R. Pellegrini, F. Scopinaro, A. Pergola, G. De Vincentis, F. Iacopi, F. de Notaristefani, A. Soluri, A. Grammatico, A. Del Guerra, Portable gamma camera for clinical use in nuclear medicine, 1996 IEEE Nuclear Science Symposium, Conference Record, Vol. 2, November 2–9 1996, Anaheim, CA, USA, 1996, p. 1170.
- [5] R. Pani, F. Scopinaro, R. Pellegrini, A. Soluri, A. Pergola, G. De Vincentis, M. Ierardi, I.N. Weinberg, *Anticancer Res.* 17 (3B) (1997) 1651.
- [6] R. Pani, R. Pellegrini, F. Scopinaro, G. De Vincentis, A. Pergola, A. Soluri, A. Corona, S. Filippi, P.L. Ballesio, A. Grammatico, *Nucl. Instr. and Meth. A* 392 (1997) 295.
- [7] R. Pani, G. De Vincentis, F. Scopinaro, R. Pellegrini, A. Soluri, I.N. Weinberg, A. Pergola, *IEEE Trans. Nucl. Sci.* NS-45 (6) (1998) 3127.
- [8] R. Pani, A. Soluri, A. Pergola, R. Pellegrini, R. Scaf , G. De Vincentis, F. Scopinaro, *IEEE Trans. Nucl. Sci.* NS-46 (3) (1999) 702.
- [9] R. Pani, A. Pergola, R. Pellegrini, G. De Vincentis, A. Soluri, S. Filippi, F. Scopinaro, G. Di Domenico, A. Del Guerra, *Nucl. Instr. and Meth. A* 392 (1997) 319.
- [10] R. Pani, R. Pellegrini, A. Soluri, G. De Vincentis, R. Scaf , A. Pergola, *Nucl. Instr. and Meth. A* 409 (1998) 524.
- [11] R. Pani, A. Soluri, R. Scaf , R. Pellegrini, A. Tati, F. Scopinaro, G. De Vincentis, T. Gigliotti, A. Festinesi, F. Garibaldi, A. Del Guerra, *Nucl. Instr. and Meth. A* 477 (2002) 509.
- [12] R. Pani, F. de Notaristefani, F. Scopinaro, R. Pellegrini, A. Pergola, A. Soluri, G. De Vincentis, T. Malatesta, F. Vittori, M. Meoni, A. Grammatico, M. Morelli, *Eur. J. Nucl. Med.* 22 (8) (1995) 876 (abstract).
- [13] F. Scopinaro, R. Pani, R. Pellegrini, G. De Vincentis, A. Pergola, A. Soluri, F. Iacopi, M. Ierardi, M. Meoni, *Q. J. Nucl. Med.* 2 (1996) (abstract).
- [14] F. Scopinaro, G. De Vincentis, R. Pani, R. Pellegrini, A. Soluri, M. Ierardi, R. Danieli, N.S. Tiberio, L. Ballesio, *Eur. J. Nucl. Med.* 24 (1997) 1048.
- [15] G. De Vincentis, F. Scopinaro, R. Pani, R. Pellegrini, A. Soluri, M. Ierardi, L. Ballesio, I.N. Weinberg, A. Pergola, *Anticancer Res.* 17 (3B) (1997) 1627.
- [16] G. De Vincentis, W. Gianni, R. Pani, M. Cacciafesta, R. Pellegrini, A. Soluri, G. Troisi, V. Marigliano, F. Scopinaro, *Breast Cancer Res. Treatment.* 48 (1998) 159.
- [17] F. Scopinaro, G. De Vincentis, R. Pani, W. Gianni, R. Pellegrini, A. Soluri, E. Di Luzio, T. Gigliotti, V. Marigliano, A. Centi Colella, *Ann. Oncol.* 9 (3) (1998) 65.
- [18] F. Scopinaro, R. Pani, G. De Vincentis, A. Soluri, R. Pellegrini, L.M. Porfiri, *Eur. J. Nucl. Med.* 26 (1999) 1279.